ARTICLE

Simulation of Sessile Water-Droplet Evaporation on Superhydrophobic Polymer Surfaces

Shuai-xia Tan, Xiao-yan Zhang, Ning Zhao, Jian Xu*

State Key Laboratory of Polymer Physics and Chemistry, Institute of Chemistry, Chinese Academy of Sciences, Beijing 100080, China

(Dated: Received on July 14, 2006; Accepted on November 8, 2006)

Evaporation of sessile water-droplets on superhydrophobic polymer surfaces has been simulated in recent research. Models based on the ellipsoidal cap geometry and spherical cap geometry, which were originally put forward to describe the profile of a droplet during its evaporation process on a solid surface with a contact angle <90°, are developed to reveal the issue with an initial contact angles larger than 150°. To verify the validity of the model, experiments on superhydrophobic polycarbonate, and fluorinated polyurethane and poly (methyl methacrylate) blend surfaces were carried out. It was observed that the change trends of contact angle and height of the droplet against evaporation time on the superhydrophobic surfaces experimentally are consistent with the simulated results by ellipsoidal and spherical cap models. The ellipsoidal cap model shows the better fits due to the shape distortions of droplets.

Key words: Evaporation, Superhydrophobicity, Contact angle, Ellipsoidal cap geometry

I. INTRODUCTION

Evaporation of liquid droplets on solid surfaces has attracted considerable attention in recent years, because understanding this process is very useful for agricultural and industrial applications such as pesticides spraying [1] and ink-jet printing [2]. Various investigations have focused on the evolution of contact angle (CA), contact area, and height of droplet against evaporation time [3-15]. By assuming the profile of a small droplet maintained a spherical cap geometry during the evaporation course, Picknett *et al.* and Shanahan *et al.* observed three distinct evaporation modes [3,4]: mode I, constant contact area with gradually diminishing contact angle ascribed to different surface roughness or chemical heterogeneity; mode II, constant contact angle with diminishing contact area attributed to less contact angle hysteresis; and mode III, both contact angle and contact area change with evaporation. Rowan *et al.* noted the height and contact angle of droplets decreased almost linearly with time for the initial CA<90° based on constant contact area model [5,6]. While in a saturated atmosphere, Erbil found the decreases of the square of contact radius and the height of droplet were linear with time and followed the constant contact angle mode [7]. They also predicted the diffusion coefficient and the difference of vapor concentration between the droplet surface and far from the droplet. More recently, McHale *et al.* developed Picknett's model to quantitatively analyze the liquid evaporation on a regularly textured surface composed of a lattice of tall pillars of SU-8 with an initial CA exceeding 150° [8]. Two cases were speculated: one was that water droplets evaporated in a pinned contact line mode (as in the constant contact area mode) at the beginning, and then the contact line receded in a stepwise fashion; the other was that evaporation proceeded in a complete pinned contact area mode after contingent droplets abruptly collapsed into the pillar structure. However, shape distortion of liquid drops often occurs due to a gravity effect [16], especially for superhydrophobic states with higher contact angle and less contact area. Moreover, hysteresis or triple-phase line tension [16-19] may also affect the shape of the droplet in the evaporation process. Therefore, the spherical cap model is somewhat insufficient for describing the droplet geometry. To characterize the profile of a droplet resting on a solid surface, a more suitable model is necessary. For a hydrophilic regime, Erbil *et al.* distinguished two principal radii of curvature at the contact line and developed a three-parameter ellipsoidal cap geometry [12,13] and a two-parameter pseudospherical cap geometry [14]. The predicted contact angle and height of droplets, in good agreement with experimental data, were both linear against evaporation time, and the ellipsoidal cap geometry showed the better fit with experimental results. For the case of a hydrophobic or superhydrophobic regime, few investigations have been reported.

Recently, superhydrophobic surfaces have aroused great research interest because of their unique properties and potential applications [20-30]. Emphasis is mostly focused on the relationship between the surface roughness and water repellency, but the influence of surface roughness on the model of water evaporation has been studied little. In this work, the ellipsoidal cap geometry and spherical cap geometry are developed to apply to water evaporation in the case of CA>90° on

*Author to whom correspondence should be addressed. E-mail: jxu@iccas.ac.cn

 ©2007 Chinese Physical Society

rough superhydrophobic polymer surfaces. The change trends of CA and the height of the droplet during evaporation as calculated from the ellipsoidal cap model are in accord with the experimental results.

II. EXPERIMENTS

The superhydrophobic PC surface, poly(methyl methacrylate) and fluorine-end-capped polyurethane blend (PMMA/FPU) surface were fabricated according to previous studies [31,32]. A drop of ultra-pure water (Millipore Biocel) with volume about 1 μL was deposited by a micro-syringe on the superhydrophobic surface, and left to evaporate in open air. The profiles of the droplet during evaporation were monitored *in situ* with a CCD at a speed of 3 frames per minute. All of the experimental measurements were conducted at 25±3 °C and a relative humidity of 35±5%, and repeated three times on different samples to validate the trends of results.

III. THEORETICAL BACKGROUND

Figure 1 depicts the profile of droplet as an ellipsoidal cap geometry.

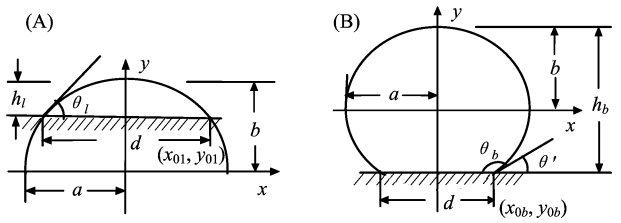

FIG. 1 The profile of droplet in the case of CA<90° in hydrophilic state (A); and in the hydrophobic state CA>90° (B). a and b are semi-axis lengths; the three parameters $\theta_l(\theta_b)$, d and h_l (h_b) are the contact angle (CA), contact diameter, and height of the droplet, respectively.

For a sessile water-droplet evaporation on a common or smooth solid surface, Rowan *et al.* had deduced the mathematic expressions based on the constant contact area mode [5]. Based on Fick's diffusion law and mass conservation, the rate of mass loss is obtained during droplet evaporation in open air as [5,12-14],

$$\rho\frac{\mathrm{d}V}{\mathrm{d}t} = -D\int\vec{\nabla}c\mathrm{d}\vec{A} = -D\int\frac{\partial c}{\partial n}\mathrm{d}A \tag{1}$$

here D is the diffusion coefficient of liquid evaporation; c is concentration and the integral of the concentration gradient covers over the spherical surface, and ρ is the density of the water. On account of the semi-axis lengths a>b and the eccentricity of the ellipse 0≤e<1, a parameter α=1−e^2=$(b/a)^2$ is defined to simplify the expression. Then h_l can be written as [12],

$$h_l(\theta_l) = \frac{d}{2}\frac{\sqrt{\alpha(\alpha+\tan^2\theta_l)}-\alpha}{\tan\theta_l} \tag{2}$$

Then useful expressions concerning the evolutions of contact angle θ_l, diameter d and height h_l of the droplet are derived as Erbil *et al.* reported [12],

$$\frac{2\alpha}{(1+\alpha)}\left(\ln h_l + \frac{{h_l}^2}{2\alpha(d/2)^2}\right) = -\frac{2\lambda(t-t_0)}{\pi(d/2)^2} \tag{3}$$

Substituting Eq.(2) into Eq.(3), the angular function $F(\theta;\alpha)$ is given as,

$$\begin{aligned} F(\theta_l;\alpha) &= \frac{2\alpha}{1+\alpha}\left[\ln\frac{\sqrt{\alpha(\alpha+\tan^2\theta_l)}-\alpha}{\tan\theta_l}\right. \\ &\quad \left. -\frac{\sqrt{\alpha(\alpha+\tan^2\theta_l)}-\alpha}{\tan^2\theta_l}+1.0\right] \\ &= -\frac{2\lambda(t-t_0)}{\pi(d/2)^2} \end{aligned} \tag{4}$$

Similar to report of Rowan *et al.* [5], λ=$2\pi D\Delta c/\rho$ has combined various constants, Δc is the difference of vapor concentration at the droplet surface assumed equal to the saturation concentration and that far from the droplet surface, and t_0 is the constant of integration.

IV. RESULTS AND DISCUSSION

In the following, we develop these expressions for a hydrophobic state with a CA>90°. The semi-axis lengths a and b can be solved (as denoted in Fig.1(B)),

$$\begin{aligned} a &= \frac{d(s+h_b)}{2\sqrt{s(s+2h_b)}}; & b &= \frac{h_b(s+h_b)}{s+2h_b} \\ y_{0b} &= -\frac{{h_b}^2}{s+2h_b}; & \theta' &= 180^\circ-\theta_b \end{aligned} \tag{5}$$

here we use s=$(d/2)\tan\theta'$ for simplifing the expression.

By combining α^2=1-e^2=$(b/a)^2$ and Eq.(5), h_b is given as,

$$h_b(\theta') = \frac{d}{2}\frac{\sqrt{\alpha(\alpha+\tan^2\theta')}+\alpha}{\tan\theta'} \tag{6}$$

To solve the Eq.(1), the volume of ellipsoidal cap V by integration is written as [12],

$$\begin{aligned} V &= \pi\int_{y_{0b}}^{b}x^2\mathrm{d}y \\ &= \frac{\pi d}{6}\frac{h(d\tan\theta'+h)}{\tan\theta'} \\ &= \frac{\pi}{6\alpha}\left(\frac{3\alpha d^2}{4}+{h_b}^2\right)h_b \end{aligned} \tag{7}$$

ISSN 1003-7713/DOI:10.1360/cjcp2007.20(2).140.5 ©2007 Chinese Physical Society

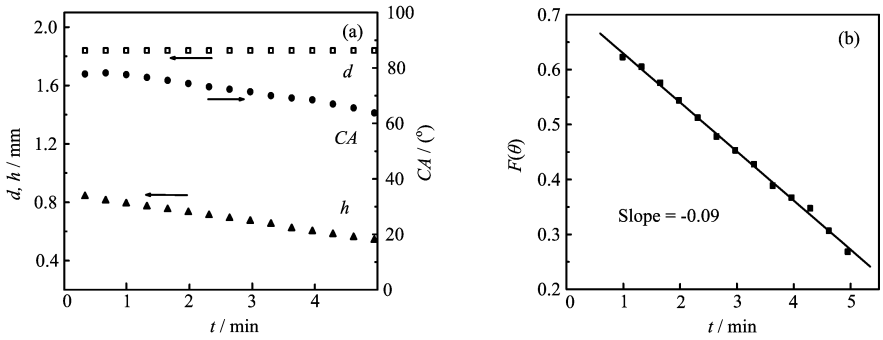

FIG. 2 (a) Evolution of CA, d and h for a water droplet with initial volume of about 1 μL on smooth PC surface in open air; (b) Plot of function $F(\theta)$ in the spherical cap model against evaporation time t.

Taking α and d to be constant, $V(\alpha, d, h)$ is implicitly differential,

$$\frac{\mathrm{d}V}{\mathrm{d}t} = \frac{\partial V}{\partial h}\frac{\partial h_b}{\partial t} = \frac{\pi}{2\alpha}\left(\frac{\alpha d^2}{4} + h_b^2\right)\frac{\mathrm{d}h_b}{\mathrm{d}t} \tag{8}$$

The surface area A by integration is given as [12],

$$A = \frac{2\pi a}{b}\int_{y_{0b}}^{b}\left[b^4 + (a^2 - b^2)y^2\right]^{1/2}\mathrm{d}y \tag{9}$$

Considering the concentration gradient as a radial outward [5-8,12-14] and distinguishing the two radii of curvature at the contact line, the gradient is written [12],

$$\frac{\partial c}{\partial n} = \frac{\Delta c}{2}\left(\frac{1}{R_1} + \frac{1}{R_2}\right) \tag{10}$$

$$\frac{1}{R_1} = \frac{ab^4}{[b^4 + (a^2 - b^2)y^2]^{3/2}} \qquad \frac{1}{R_2} = \frac{b^2}{a[b^4 + (a^2 - b^2)y^2]^{1/2}} \tag{11}$$

Then, combining Eqs.(1) and (9-11), the right side of Eq.(2) is obtained as,

$$-\frac{2\pi D\Delta c}{\rho}h_b\left[\frac{1}{2} + \frac{a}{2h_b e}\left(\tan^{-1}\frac{ea}{b} + \tan^{-1}\frac{y_{0b}ea}{b^2}\right)\right] \cong -\frac{2\alpha}{1+\alpha}\lambda h_b \tag{12}$$

here the inverse tangent function can be expanded as an infinite series: $\tan^{-1}x = x - \frac{x^3}{3} + \frac{x^5}{5} - \cdots$ and we neglect the higher order terms.

Substituting Eq.(8) and Eq.(12) into Eq.(1) and integrating gives,

$$\begin{aligned} F(\theta';\alpha) &= \frac{2\alpha}{1+\alpha}\left[\ln\frac{\sqrt{\alpha(\alpha+\tan^2\theta')}+\alpha}{\tan\theta'} + \frac{\sqrt{\alpha(\alpha+\tan^2\theta')}+\alpha}{\tan^2\theta'} + 1.0\right] \\ &= -\frac{2\lambda(t-t_0)}{\pi(d/2)^2} \end{aligned} \tag{13}$$

When α=1.0, and the eccentricity e=0, Eq.(13) reduces to the spherical cap expression,

$$\begin{aligned} F(\theta') &= -\ln\left(\tan\frac{\theta'}{2}\right) + \frac{1+\cos\theta'}{\sin^2\theta'} \\ &= -\frac{2\lambda(t-t_0)}{\pi(d/2)^2} \end{aligned} \tag{14}$$

It is noted that substituting the CA with θ_b=180°$-\theta'$, the above equation will resemble the one Rowan *et al.* derived [5,12].

$$\begin{aligned} F(\theta_b) &= \ln\left(\tan\frac{\theta'}{2}\right) + \frac{1-\cos\theta_b}{\sin^2\theta_b} \\ &= -\frac{2\lambda(t-t_0)}{\pi(d/2)^2} \end{aligned} \tag{15}$$

To check the extended ellipsoidal model, the behaviors of water-droplet evaporation on superhydrophobic polymer surfaces were investigated. In order to fix the unknown parameters, we conducted a common experiment on smooth hydrophilic PC surface. Fig.2(a) shows the evolutions of CA, d, and h of a droplet for a water droplet about 1 μL in volume at the initial stage of evaporation on this surface. The contact diameter holds constant at 1.84 mm. Due to small mass and large contact area, it is safe to assume the shape of the sessile droplet to be a spherical cap. According to Eq.(12), we plot the angular function $F(\theta)$ against time t in Fig.2(b). The fitting curve shows a good agreement with the expected linearity, which conforms to the previous report [5]. By rearranging Eq.(12) as,

$$\begin{aligned} F(\theta) &= -\frac{2\lambda}{\pi(d/2)^2}t + \frac{2\lambda}{\pi(d/2)^2}t_0 \\ &= -\frac{2\lambda(t-t_0)}{\pi(d/2)^2} \end{aligned} \tag{16}$$

From the slope of $F(\theta)$ against time t, $4D\Delta c/\rho(d/2)^2$ =0.09, thus $D\Delta c$ is obtained as 317 μg/m s. In our experimental condition, the temperature and relative humidity are 25±3 °C and 35±5%, respectively. Δc is

ISSN 1003-7713/DOI:10.1360/cjcp2007.20(2).140.5 ©2007 Chinese Physical Society

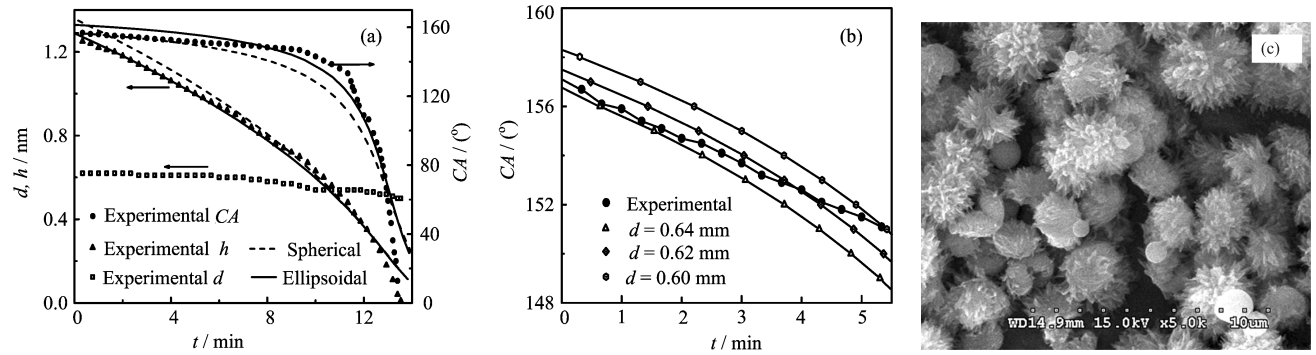

FIG. 3 (a) Evolution of CA, d and h for a water droplet of initial volume about 1 μL on superhydrophobic PC surface in open air. The scatter lines are the fitting curves of CA and h against evaporation time t based on ellipsoidal and spherical models; (b) Time dependence of CA from experimental data and calculated data with different radii; (c) SEM image of superhydrophobic PC surface with micro-nano-binary structure.

about 15 g/m^3 and D is 2.1×10^{-5} m^2/s, compared with an ideal expected value of 2.6×10^{-5} m^2/s.

In respect of the superhydrophobic PC surface, Fig.3(a) indicates the dependence of CA, d and h of the droplet against time t in the course of evaporation. During the initial stage, the CA and d reduce little, whereas h diminishes incessantly. After a long time, CA reduces rapidly until it vanishes, while d remains approximately constant. Figure 3(c) gives its SEM image with micro-nano-binary structure. Due to such a special hierarchical structure, a great amount of air trapped between the solid and water interface dramatically decreases the solid-liquid contact area, so the water-repellent surface is easily produced with an initial CA greater than 150° [20-30]. However, there is still some contact at the solid-liquid interface, and the interaction between the water and chemical composition may lead to the pinned three-phase contact line [15,29]. As a water droplet tends to shrink on this surface, a liquid-solid contact point must pass across the neighboring liquid-gas contact area and shift to another adjacent liquid-solid contact point [33,34]. But the evaporation process is so slow and gentle that it is hard to overcome the energy barrier for the three-phase line transition. Moreover, the gravity of the droplet could induce the water to penetrate the micro-cavities and thus increase the solid-liquid interface and adhesion [30].

According to the ellipsoidal and spherical models of Eqs.(2)-(4) and (13)-(15), the evolutions of CA and h are simulated, as shown in Fig.3(a). The diameter d and ratio b/a used for analysis are the average values of all measured data over the whole period, owing to approximately constant behavior in the entire evaporation process. The eccentricity e is set to 0.5. It is seen that the simulated change trends of contact angle and height of droplets are consistent with the experimental results. The data from the ellipsoidal cap model fits the experimental values better. This confirms that the extended ellipsoidal cap model is suitable to eliminate the distortion effects in the course of evaporation. However, the results also show that both the first and last stages deviate from the experimental values, even if the spherical model exhibits a better fit at the beginning. To interpret the differences, we further analyze these values. The contact diameter is assumed to be constant, but actually it does contract a little. This means the average diameter values we chose is smaller than the actual data at the initial stage in the whole simulated evaporation process. This makes the calculated data CA larger than the experimental values. Figure 3(b) shows the CA evolution $vs.$ t with different diameters. It is seen that the fitting curves match experimental results more perfectly as the d of water droplet decreases. Similarly, for the spherical cap model, the calculated data will be smaller than the actual value. On the other hand, by rearranging Eq.(15) as,

$$t = t_0 - \frac{\rho(d/2)^2}{4D\Delta c}F(\theta) \tag{17}$$

It is clearly that $F(\theta)$ is larger than zero for the hydrophobic state, and the average d, which is a little smaller than the actual values, may shift the calculated data to a smaller t. The last stage is more complex. As the contact angle decreases, the liquid-vapor interfacial tension directed horizontally towards the center of the drop will increase. It is difficult for a static radius to be maintained. Finally, the drop disappears and d attenuates to zero. In practice, Eq.(17) also reveals that the curve should terminate at time t_0, but $F(\theta)$ is less than zero at the last stage, and the average d, a little larger than the actual one, will makes the calculated data shift to larger t.

We further study the water evaporation on superhydrophobic FPU/PMMA surfaces. The surface is covered by a low surface energy fluorinated compound and also has a hierarchical surface structure on micro- and nano-scale. Figure 4 shows the changes of d, h and CA for a sessile water-droplet during the evaporation measured experimentally and calculated from the ellipsoidal cap model. Although d has diminished a little, the CA

ISSN 1003-7713/DOI:10.1360/cjcp2007.20(2).140.5 ©2007 Chinese Physical Society

change trends of experimental and simulated values are still consistent, analogous to the superhydrophobic PC surface. From these results, it seems believable that the CA decreases only a little for a long initial stage and then decreases sharply in the process of evaporation on a superhydrophobic surface, which is mainly caused by the special surface structure but also has a little correlation with the surface chemical composition.

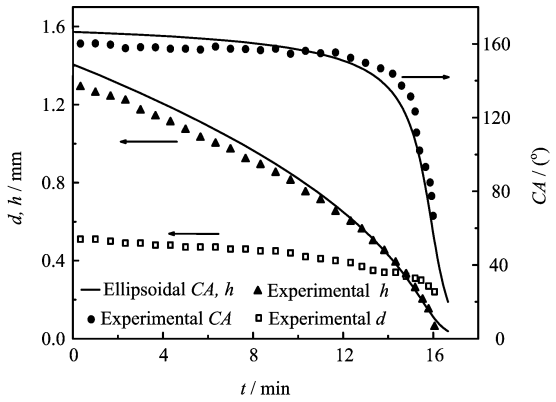

FIG. 4 Evolution of CA, d and h for a water droplet of initial volume about 1 μL on superhydrophobic FPU/PMMA surface in open air. The solid lines are fitting curves of CA and h against t based on the ellipsoidal model.

V. CONCLUSION

The two-parameter (contact angle CA, diameter of droplets d) ellipsoidal cap model and spherical cap model, which were originally developed to describe the evaporation of a sessile water drop on a solid surface with a CA less than 90°, are adapted and applied to characterize the superhydrophobic surface with an initial CA larger than 150° based on the constant contact area mode. The data obtained from evaporation experiments on the superhydrophobic polymer surfaces fit the models well. It is observed that the ellipsoidal cap model conforms to the experimental values better than the spherical cap model because of the effects of gravity, triple-phase line tension, etc. Our results show that the surface roughness not only has a great effect on the surface wetting behavior, but also has a profound influence on the mode of water evaporation on the surface.

VI. ACKNOWLEDGMENTS

This work was supported by the National Natural Science Foundation of China (No.50373049, No.50521302 and No.50425312), 973 Program (No.2005CCA00800) and the Innovation Project of Chinese Academy of Sciences.

[1] R. Reichman, Y. Mahrer and R. Wallach, Environ. Sci. Technol. **34**, 1321 (2000).
[2] S. Magdassi and M. Ben-Moshe, Langmuir **19**, 939 (2003).
[3] R. G. Picknett and R. Bexon, J. Colloid Interface Sci. **61**, 336 (1977).
[4] C. Bourgès-Monnier and M. E. R. Shanahan, Langmuir **11**, 2820 (1995).
[5] S. M. Rowan, M. I. Newton and G. McHale, J. Phys. Chem. **99**, 13268 (1995).
[6] G. McHale, S. M. Rowan, M. I. Newton and M. K. Banerjee, J. Phys. Chem. B **102**, 1964 (1998).
[7] H. Y. Erbil and Y. Avci, Langmuir **18**, 5113 (2002).
[8] G. McHale, S. Aqil, N. J. Shirtcliffe, M. I. Newton and H. Y. Erbil, Langmuir **21**, 11053 (2005).
[9] M. Cachile, O. Bénichou, C. Poulard and A. M. Cazabat, Langmuir **18**, 8070 (2002).
[10] C. Poulard, G. Guéna, A. M. Cazabat, A. Boudaoud and M. B. Amar, Langmuir **21**, 8226 (2005).
[11] H. Hu and R. G. Larson, J. Phys. Chem. B **106**, 1334 (2002).
[12] H. Y. Erbil and R. A. Meric, J. Phys. Chem. B **101**, 6867 (1997).
[13] H. Y. Erbil, J. Adhes. Sci. Technol. **13**, 1375 (1999).
[14] R. A. Meric and H. Y. Erbil, Langmuir **14**, 1915 (1998).
[15] X. Zhang, S. Tan, N. Zhao, X. Guo, X. Zhang, Y. Zhang and J. Xu, Chem. Phys. Chem. **7**, 2067 (2006).
[16] H. Sakai and T. Fujii, J. Colloid Interface Sci. **210**, 152 (1999).
[17] M. Miyama, Y. X. Yang, T. Yasuda, T. Okuno and H. K. Yasuda, Langmuir **13**, 5494 (1997).
[18] C. W. Extrand, Langmuir **18**, 7991 (2002).
[19] H. Y. Erbil, G. McHale, S. M. Rowan and M. I. Newton, Langmuir **15**, 7378 (1999).
[20] A. Marmur, Langmuir **20**, 3517 (2004).
[21] Z. Yoshimitsu, A. Nakajima, T. Watanabe and K. Hashimoto, Langmuir **18**, 5818 (2002).
[22] R. Blossey, Nat. Mater. **2**, 301 (2003).
[23] N. J. Shirtcliffe, G. McHale, M. I. Newton, G. Chabrol and C. C. Perry, Adv. Mater. **16**, 1929 (2004).
[24] L. Feng, S. Li, Y. Li, H. Li, L. Zhang, J. Zhai, Y. Song, B. Liu, L. Jiang and D. Zhu, Adv. Mater. **14**, 1857 (2002).
[25] H. Duan, C. Bai, H. Wang, L. Zhao and H. Zhao, New Chem. Mat. **34**, 55 (2006).
[26] X. F. Gao, L. Jiang, Physics **35**, 559 (2006).
[27] C. H. Su, Y. Xiao, Z. Cui, C. G. Liu, Q. J. Wang and Q. M. Chen, Chin. J. Inorg. Chem. **22**, 785 (2006).
[28] S. H. Li, L. Feng, H. J. Li, J. Zhai, Y. L. Song, L. Jiang and D. B. Zhu, Chem. Res. Chin. Univ. **24**, 340 (2003).
[29] X. Song, J. Zhai, Y. Wang and L. Jiang, J. Phys. Chem. B **109**, 4048 (2005).
[30] A. Dupuis and J. M. Yeomans, Langmuir **21**, 2624 (2005).
[31] N. Zhao, J. Xu, Q. D. Xie, L. H. Weng, X. L. Guo, X. L. Zhang and L. H. Shi, Macromol. Rapid Commun. **26**, 1075 (2005).
[32] Q. D. Xie, Xu J., L. Feng, L. Jiang, W. Tang, X. Luo and C. C. Han, Adv. Mater. **16**, 302 (2004).
[33] F. G. Robert, *Contact Angle, Wettability, and Adhesion*, Washington: American Chemical Society, 112 (1964).
[34] Y. T. Cheng and D. E. Rodak, Appl. Phys. Lett. **87**, 194112 (2005).

ISSN 1003-7713/DOI:10.1360/cjcp2007.20(2).140.5 ©2007 Chinese Physical Society